Atmospheric
Chemistry
and Physics

Highly oxygenated organic molecules produced by the oxidation of benzene and toluene in a wide range of OH exposure and NO$_x$ conditions

Xi Cheng[1], **Qi Chen**[1], **Yong Jie Li**[2], **Yan Zheng**[1], **Keren Liao**[1], and **Guancong Huang**[1]

[1]State Key Joint Laboratory of Environmental Simulation and Pollution Control, BIC-ESAT and IJRC, College of Environmental Sciences and Engineering, Peking University, Beijing, China
[2]Department of Civil and Environmental Engineering, Faculty of Science and Technology, University of Macau, Taipa, Macau SAR, China

Correspondence: Qi Chen (qichenpku@pku.edu.cn) and Yong Jie Li (yongjieli@um.edu.mo)

Abstract. Oxidation of aromatic volatile organic compounds (VOCs) leads to the formation of tropospheric ozone and secondary organic aerosol, for which gaseous oxygenated products are important intermediates. We show, herein, the experimental results of highly oxygenated organic molecules (HOMs) produced by the oxidation of benzene and toluene in a wide range of OH exposure and NO$_x$ conditions. The results suggest that multigeneration OH oxidation plays an important role in the product distribution, which likely proceeds more preferably via H subtraction than OH addition for early generation products from light aromatics. More oxygenated products present in our study than in previous flow tube studies, highlighting the impact of experimental conditions on product distributions. The formation of dimeric products, however, was suppressed and might be unfavorable under conditions of high OH exposure and low NO$_x$ in toluene oxidation. Under high-NO$_x$ conditions, nitrogen-containing multifunctional products are formed, while the formation of other HOMs is suppressed. Products containing two nitrogen atoms become more important as the NO$_x$ level increases, and the concentrations of these compounds depend significantly on NO$_2$. The highly oxygenated nitrogen-containing products might be peroxyacyl nitrates, implying a prolonged effective lifetime of RO$_2$ that facilitates regional pollution. Our results call for further investigation on the roles of high-NO$_2$ conditions in the oxidation of aromatic VOCs.

1 Introduction

Atmospheric oxidation of volatile organic compounds (VOCs) are crucial in the formation of tropospheric ozone (O$_3$) and secondary organic aerosol (SOA; Calvert et al., 2015; Seinfeld and Pandis, 2016). Enormous studies have been conducted for the O$_3$ formation potentials and SOA yields of light aromatic VOCs such as benzene and toluene (Calvert et al., 2002; Atkinson and Arey, 2003; Ziemann and Atkinson, 2012). The peroxy radicals (either RO$_2$ or HO$_2$) that are generated from the oxidation process convert NO to NO$_2$. Ground-state oxygen atoms O(^{3}P) are produced through the photolysis of NO$_2$, and the reaction between the O(^{3}P) and O$_2$ is the main source of tropospheric O$_3$ (Calvert et al., 2015). The oxygenated organic products, on the other hand, may form SOA through either nucleation or condensation with various mass yields, depending on the structure of the precursors and the NO$_x$ ($=$ NO $+$ NO$_2$) level (Ng et al., 2007; Li et al., 2016). Therefore, for both O$_3$ and SOA formation via VOC oxidation, NO$_x$ plays a critical role (Atkinson, 2000; Sato et al., 2012; Tsiligiannis et al., 2019; Garmash et al., 2020).

OH-initiated oxidation of light aromatics occurs mainly via OH addition, with about 90 % of preference (Calvert et al., 2002; Wu et al., 2014; Schwantes et al., 2017). As described in Sect. S1 in the Supplement, the formation of bicyclic peroxy radicals (BPRs) is central to aromatic oxidation in the absence of NO$_x$. Significant fractions of the oxidation (e.g., 0.35 for benzene and 0.65 for toluene) may lead

to the formation of BPRs (Scheme S1 in the Supplement; Birdsall et al., 2010), followed by further reactions to form highly oxygenated organic molecules (HOMs; Crounse et al., 2013; Ehn et al., 2014; Berndt et al., 2016; Bianchi et al., 2019). The fate of the BPRs has been recently investigated by using a time-of-flight chemical ionization mass spectrometer (TOF-CIMS), which is suitable for measuring HOMs. The TOF-CIMS measurements show that major products for the reactions between BPRs and HO_2/RO_2 in the absence of NO_x include carbonyls, alcohols, hydroperoxides, dimers, and alkoxy (RO) radicals (Birdsall et al., 2010; Wang et al., 2017; Molteni et al., 2018; Zaytsev et al., 2019b; Garmash et al., 2020). The BPR-derived products that still possess the bicyclic skeleton are considered as being the major ring-retaining products from the oxidation of light aromatics (Zaytsev et al., 2019b). The decomposition of RO radicals may lead to fragmented products such as di-carbonyls and epoxides (Yu and Jeffries, 1997; Yu et al., 1997; Arey et al., 2009; Zaytsev et al., 2019b). The formation of HOMs may involve multistep auto-oxidation and multigeneration OH reaction (Zaytsev et al., 2019b; Garmash et al., 2020; Y. Wang et al., 2020). Yet, it is still unclear whether the formation of HOMs is controlled by multistep auto-oxidation or multigeneration OH oxidation.

Conditions of flow tube or smog chamber experiments have covered various conditions of OH concentrations (10^4 to 10^{11} $mol\,cm^{-3}$) and residence times (10 s to 1 h; Wang et al., 2017; Molteni et al., 2018; Garmash et al., 2020). Extrapolation of these results to tropospheric conditions requires further investigations under a wide range of NO_x levels. NO_x are rich in urban environments and compete with HO_2 and RO_2 for the termination of RO_2 radicals (Calvert et al., 2002; Seinfeld and Pandis, 2016). Early studies show a strong dependence of SOA mass yields on NO_x, owing to the formation of more volatile products through the termination of RO_2 by NO (Ng et al., 2007; Sato et al., 2012). There are also a few recent studies on the gaseous oxygenated products from aromatic oxidation in the presence of NO_x (Tsiligiannis et al., 2019; Garmash et al., 2020; Y. Wang et al., 2020). Garmash et al. (2020) found that nitrated phenols (NPs) contribute significantly to the gaseous nitrogen-containing HOMs produced by the benzene oxidation in the presence of NO_x. Tsiligiannis et al. (2019) show the prevalent formation of organic nitrates (ONs) from 1,3,5-trimethylbenzene (TMB) oxidation, especially for atmospherically relevant $[NO_x]:[VOC]$ ratios greater than 1. In addition to ONs, Y. Wang et al. (2020) show the elevated formation of dinitrates from the oxidation of TMB isomers in the presence of NO_x. In general, the formation of these nitrogen-containing products suppresses the formation of other HOMs (Tsiligiannis et al., 2019; Garmash et al., 2020; Y. Wang et al., 2020). However, the dependence of product distributions on NO_x conditions (e.g., $[NO_x]:[VOC]$ or $[NO_2]:[NO]$ ratios) remains largely unclear.

In this study, we investigate the production of gaseous HOMs from the OH-initiated oxidation of benzene and toluene in an oxidation flow reactor (OFR) by using nitrate adduct TOF-CIMS (NO_3^--TOF-CIMS). A wide range of OH exposure and NO_x conditions are studied. Distributions and molar yields of key products are investigated. Kinetic analysis helps in inferring the possible formulas of nitrogen-containing HOMs.

2 Experimental section

2.1 Oxidation flow reactor

The oxidation experiments are conducted in a 13.3 L Aerodyne Research Inc. potential aerosol mass (PAM) OFR reactor. The schematic of the experimental setup and the example experimental sequence are shown in Figs. S1 and S2 in the Supplement, respectively. The OFR was operated in two continuous flow modes named OFR254-5 and OFR254-5–iN$_2$O (Lambe et al., 2017; Peng et al., 2018). For the OFR254-5 mode, the inside UV lamps emit photons at 254 nm to generate OH radicals in the reactor via the reaction of $O(^1D) + H_2O \rightarrow 2OH$. An outside UV lamp produces O_3 and leads to about 5 ppm (parts per million) of O_3 in the OFR. For the OFR254-5–iN$_2$O mode, N_2O (99.5 %) is injected into the OFR to achieve N_2O mixing ratios of 1.1 % (OFR254-5–iN$_2$O1.1) and 4.4 % (OFR254-5–iN$_2$O4.4). NO and NO_2 are then formed by the reaction $O(^1D) + N_2O \rightarrow 2NO$, followed by the reaction $NO + O_3 \rightarrow NO_2 + O_2$ (Lambe et al., 2017). The conditions for OFR254-5 are considered as being low-NO_x, whereas the latter are high-NO_x. Under each of these three sets of experiments, OH exposure and NO_x levels were varied by ramping the voltage of the UV lamps in the OFR. The total flow rate was about 8.4 $L\,min^{-1}$, resulting in a mean residence time of 95 s in the OFR. Relative humidity (RH) in the OFR was about 20 % to 55 % at $25 \pm 2\,^\circ C$, corresponding to H_2O mixing ratios of about 0.7 % to 1.5 %. Details about the experimental setup are provided in Sect. S2 in the Supplement.

In total, 28 experiments were conducted for initial mixing ratios of 110 ppb (parts per billion) benzene and 50 ppb toluene. Table S1 in the Supplement lists the experimental conditions and the measured and derived quantities for all experiments. The concentrations of reactive species such as OH, HO_2, NO, and NO_2 were estimated by an OFR-based photochemical box model (PAMchem; Lambe et al., 2017). The box model simulations are described in detail in Sect. S2, for which calibration experiments with SO_2 were conducted to constrain the actinic flux at 254 nm (Fig. S3 in the Supplement). Briefly, the model suggests OH exposure of about 1.1×10^{11} to 2.5×10^{12} $mol\,cm^{-3}\,s$ for our experiments, corresponding to equivalent photochemical age of 0.8 to 19.3 d, with a mean OH concentration of 1.5×10^6 $mol\,cm^{-3}$. For high NO_x experiments, the OFR exit NO and NO_2 concentra-

tions were 0.2 to 5.1 ppb and 15.8 to 231.4 ppb, respectively, leading to $[NO_x] : [VOC]$ ratios of 0.2 to 2.2 for benzene and 0.4 to 4.7 for toluene. The OFR-based photochemical box simulations show that the aromatic oxidation reactions in our experimental conditions were dominated by OH rather than O_3 (Lambe et al., 2011; Peng et al., 2016). Similar to other OFR studies, we think the reaction rates of O_3 with oxidation products that contain double bounds are likely slower compared to that of OH (Molteni et al., 2018; Y. Wang et al., 2020). The NO_3 concentrations in the OFR range from 0.01 to 0.09 ppb. The general reaction rate of RO_2 with OH is 1 order of magnitude greater than that with NO_3 under our experimental conditions (Jenkin et al., 2019). For such rates, the NO_3 reactions with HOM products might be minor. The NO_3 oxidation of phenols, however, may contribute efficiently to the formation of nitrated phenols in the OFR because of the high branching ratio.

2.2 Chemical characterization

HOMs were characterized by an Aerodyne Research Inc. NO_3^--TOF-CIMS. Details about the instrument operation and data analysis are described elsewhere (Cheng et al., 2021). Briefly, mass calibration was performed on the reagent ions and selected Teflon-related ions, which covers the m/z range of 62 to 676, with mass accuracies of less than 10 ppm. The non-production ions were identified by positive matrix factorization (PMF) analysis and were removed from the analysis (Fig. S4 in the Supplement). The $HNO_3NO_3^-$ adduct ions were identified by the signal correlations between the NO_3^- adduct and $HNO_3NO_3^-$ adduct ions and were removed from the analysis (Fig. S5 in the Supplement). Only NO_3^- adduct ions are presented herein. The background signals of individual ions were determined on the basis of the measurements made without the injection of VOCs (Fig. S2). Because of the lack of standards, we applied the calibration factor of 4-nitrophenol (i.e., 0.0020 ncps ppt^{-1} (normalized counts per second per parts per trillion) or 1.66×10^{10} mol cm^{-3}) to HOMs, which is similar to the commonly used calibration factors of H_2SO_4 (i.e., 1.62×10^{10} mol cm^{-3} for our instrument herein and 1.89×10^{10} mol cm^{-3} reported by Jokinen et al., 2012) and perfluoroheptanoic acid (i.e., 1.6×10^{10} mol cm^{-3} as reported by Ehn et al., 2014). All calibration factors are corrected by wall losses. Ehn et al. (2014) reported a ±50 % of uncertainty. For our experiments, we estimate an uncertainty of 42 % on the basis of nitrated phenol calibrations (Cheng et al., 2021). In some experiments, the VOC precursors and less-oxygenated gaseous products were monitored by an IONICON proton transfer reaction-quadrupole interface time-of-flight mass spectrometer (PTR-QiTOF). The instrument operation and data analysis have been described previously (Huang et al., 2019). The measurements have a total uncertainty of about 21 %. Particle size distributions were measured by a scanning mobility particle sizer (SMPS; TSI Incorporated; model no. 3938). The SOA
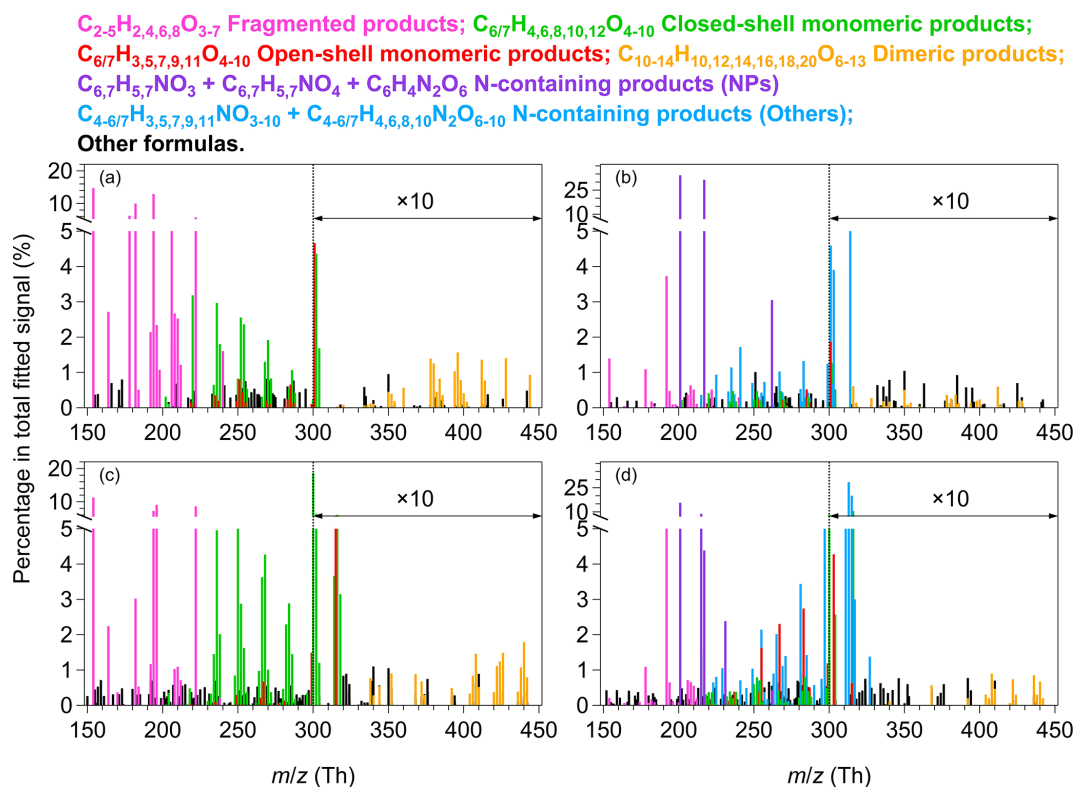
mass concentrations are measured by an Aerodyne long time-of-flight soot particle aerosol mass spectrometer (LTOF-SP-AMS) for the calculation of condensation sink in wall loss corrections of HOMs (Zheng et al., 2020).

3 Results and discussion

3.1 Product categories

Figure 1 shows the mass spectra of gaseous oxygenated products produced by benzene and toluene oxidation in typical low- and high-NO_x experiments. The fitted ion peaks are categorized into fragmented products, open-shell monomeric products, closed-shell monomeric products, and dimeric products, as well as nitrogen-containing products when NO_x is present. The proposed product categories are based on traditional understanding and recent mechanistic developments of aromatic oxidation (Wang et al., 2017; Mentel et al., 2015; Molteni et al., 2019). In benzene and toluene (C_xH_y) oxidation by OH radicals, the addition of OH and two O_2 molecules leads to the formation of BPR $C_xH_{y+1}O_5$, which increase the molecular composition by one H atom and five oxygen atoms. The BPR $C_xH_{y+1}O_5$ can undergo further autoxidation and forms radicals with the formula $C_xH_{y+1}O_7$. Autoxidation of RO_2 radicals involves intramolecular hydrogen shifts to the peroxide group from other carbon atoms and the subsequent addition of oxygen to the produced carbon-centered radicals. The H shift itself does not modify the molecular composition, but O_2 addition increases the oxygen content by an even number. Besides, BPR $C_xH_{y+1}O_5$ can form termination products of carbonyls ($C_xH_yO_4$), alcohols ($C_xH_{y+2}O_4$), hydroperoxides ($C_xH_{y+2}O_5$), dimers, and nitrogen-containing compounds. Notably, product distributions are affected by the numbers of the generation of the auto-oxidation pathway and the H shift reaction rates. Some product formulae may involve multiple pathways, as discussed later in Sect. 3.2, for which additional information (e.g., collision induced dissociation experiments) may be helpful to further explore possible structures of the HOM molecules (Zaytsev et al., 2019a).

Tables S2–S3 in the Supplement list the corresponding peak lists and relative signal contributions of major products in each category for the low- and high-NO_x experiments in Fig. 1. The fragmented products are the most abundant category under low-NO_x conditions. They have carbon numbers less than their precursors, possibly indicating ring opening or scission, presumably from RO radicals (Zaytsev et al., 2019b). In addition, fragmented products can be formed through CO elimination from an acyl radical (Rissanen et al., 2014), splitting CO_2 from an RO radical (Garmash et al., 2020), or dealkylation (Birdsall and Elrod, 2011). In this study, $C_2H_4O_4$ shows the highest signal intensity in the fragmented category under low-NO_x conditions. $C_4H_4O_5$ and $C_5H_4O_6$ are the other two abundant common products

C$_{2-5}$H$_{2,4,6,8}$O$_{3-7}$ Fragmented products; C$_{6/7}$H$_{4,6,8,10,12}$O$_{4-10}$ Closed-shell monomeric products;
C$_{6/7}$H$_{3,5,7,9,11}$O$_{4-10}$ Open-shell monomeric products; C$_{10-14}$H$_{10,12,14,16,18,20}$O$_{6-13}$ Dimeric products;
C$_{6,7}$H$_{5,7}$NO$_3$ + C$_{6,7}$H$_{5,7}$NO$_4$ + C$_6$H$_4$N$_2$O$_6$ N-containing products (NPs)
C$_{4-6/7}$H$_{3,5,7,9,11}$NO$_{3-10}$ + C$_{4-6/7}$H$_{4,6,8,10}$N$_2$O$_{6-10}$ N-containing products (Others);
Other formulas.

Figure 1. Mass spectra of HOM products measured by the NO$_3^-$-TOF-CIMS for experiment nos. 2, 11, 16, and 26 in Table S1. **(a)** Benzene and OFR254-5. **(b)** Benzene and OFR254-5–iN$_2$O4.4. **(c)** Toluene and OFR254-5. **(d)** Toluene and OFR254-5–iN$_2$O4.4. The reagent ion NO$_3^-$ is omitted from the molecular formulas, whereas the m/z values refer to the mass-to-charge ratios of the fitted ions, with NO$_3^-$. The relative intensities of ions having $m/z \geq 300$ are multiplied by 10.

in this category. Under high-NO$_x$ conditions, C$_4$H$_2$O$_5$ is the most abundant common product for benzene and toluene oxidation. Many of the fragmented products have been detected in SOA (Gallimore et al., 2011; Gowda and Kawamura, 2018).

The ring-retaining HOM monomers may have even (closed shell) or odd (open shell) hydrogen numbers (Molteni et al., 2018; Zaytsev et al., 2019b; Garmash et al., 2020). With relatively large carbon numbers, the RO$_2$ radicals generally have lifetimes of seconds that are much longer than the RO radicals of $< 10^{-4}$ s (Orlando et al., 2003; Seinfeld and Pandis, 2016; Zhao et al., 2018). The open-shell monomeric products observed by the NO$_3^-$-TOF-CIMS in this study are, therefore, more likely RO$_2$ radicals rather than RO radicals. Under low-NO$_x$ conditions, the BPRs have relatively low signal intensities (0.1 %). Products that are presumably formed by further auto-oxidation of BPRs, such as C$_6$H$_7$O$_7$ and C$_6$H$_7$O$_9$ for benzene (or C$_7$H$_9$O$_7$ and C$_7$H$_9$O$_9$ for toluene), have much greater signal intensities compared with the BPRs, especially for the O$_9$ products. Other open-shell monomeric products with two fewer hydrogen atoms (e.g., H$_5$ for benzene and H$_7$ for toluene) or with an even number of oxygen atoms (e.g., O$_6$ or O$_{10}$) are also present.

Under high-NO$_x$ conditions, the main open-shell monomers are the O$_9$ products, which is similar to the low-NO$_x$ case.

Among the closed-shell monomeric products produced by benzene oxidation, C$_6$H$_6$O$_{5-10}$ and C$_6$H$_8$O$_{5-10}$ with one oxygen atom apart show relatively high signal intensities, and C$_6$H$_6$O$_5$ and C$_6$H$_6$O$_6$ are the most abundant ones. C$_6$H$_6$O$_5$ and C$_6$H$_6$O$_6$ might be carbonyl products from the termination of C$_6$H$_7$O$_6$ and C$_6$H$_7$O$_7$ by HO$_2$ or RO$_2$ (Zaytsev et al., 2019b; Garmash et al., 2020). C$_6$H$_7$O$_6$ is probably formed by the ring breakage of the bicyclic alkoxy radical followed by the 1,5 aldehydic alkoxy H shift reactions (Xu et al., 2020) which involve the RO pathway, as described in detail in Sect. S3 of the Supplement. For other products formed by the termination reactions of BPR with HO$_2$ or RO$_2$, bicyclic hydroperoxide (C$_6$H$_8$O$_5$), carbonyl (C$_6$H$_6$O$_4$), and alcohol (C$_6$H$_8$O$_4$) have relatively small signals, whereas the products that may involve two or three steps of auto-oxidation (e.g., C$_6$H$_8$O$_7$ and C$_6$H$_8$O$_9$) have greater signal intensities. BPRs (i.e., C$_6$H$_7$O$_5$ from benzene oxidation and C$_7$H$_9$O$_5$ from toluene oxidation) can undergo unimolecular isomerization reactions to form more oxidized peroxy radicals, which compete with bimolecular reactions (Wang et al., 2017). The relative greater signal intensities of ring-retaining O$_7$ or O$_9$ HOM monomers compared with O$_{<6}$ ones sug-

gest that the termination of RO_2 by HO_2 and the phenol oxidation pathway are perhaps relatively less important than the auto-oxidation pathway under experimental conditions herein (Calvert et al., 2002; Schwantes et al., 2017; Garmash et al., 2020). Similarly, for toluene oxidation, the bicyclic hydroperoxide ($C_7H_{10}O_5$) shows lower signals than $C_7H_{10}O_7$ and $C_7H_{10}O_9$ that may be associated with multiple steps of auto-oxidation. $C_7H_8O_6$ and $C_7H_8O_7$ are the main closed-shell monomers that might be carbonyls that are produced by the termination of $C_7H_9O_7$ and $C_7H_9O_8$ by HO_2 or RO_2, respectively. The formation of $C_7H_8O_7$ may also be explained by the RO pathway, similar to $C_6H_6O_5$ (Sect. S3). The RO pathway, if it occurs, may potentially lead to various products with significant signals, which remains largely overlooked in studies of aromatic oxidation (Xu et al., 2020).

The other two categories are dimeric and nitrogen-containing products. In our study, the ion intensities of dimeric products with odd hydrogen atoms are low. We, therefore, focus on the dimeric products with even hydrogen atoms. Under low-NO_x conditions, dimeric products with 8–14 even oxygen atoms are clearly present. $C_{12}H_{14}O_8$ and $C_{14}H_{18}O_8$ are perhaps formed via self-reactions of the BPRs for benzene and toluene, respectively. The distribution of dimeric products is in line with the monomeric open-shell and closed-shell products. We observe a number of dimeric products with odd oxygen numbers that are perhaps produced by cross-reactions of odd and even oxygen RO_2 (Molteni et al., 2018; Garmash et al., 2020). The presence of NO_x results in the formation of nitrogen-containing products with one or two nitrogen atoms, and the signal abundances of all other oxygenated products are much lower than the case of low-NO_x experiments. Such a suppression has been reported previously (Tsiligiannis et al., 2019; Garmash et al., 2020; Y. Wang et al., 2020; Mehra et al., 2020). The nitrogen-containing products are expected to be organic nitrates or nitrated phenols. For benzene oxidation, $C_6H_5NO_3$, $C_6H_5NO_4$, and $C_6H_4N_2O_6$ are the most abundant, which are plausibly nitrophenol, nitrocatechol, and dinitrocatechol, respectively. For toluene, $C_6H_5NO_3$ (nitrophenol), $C_6H_5NO_4$ (nitrocatechol), $C_7H_7NO_3$ (methylnitrophenol), and $C_7H_7NO_4$ (methylnitrocatechol) are the main tentatively assigned nitrated phenols. Significant secondary production of these compounds from aromatic oxidation have been observed in urban Beijing (Cheng et al., 2021). Other products, such as $C_6H_7NO_8$, $C_6H_7NO_9$, and $C_7H_9NO_8$, are most likely organic (peroxy) nitrates. Schemes S2 and S3 in the Supplement give examples of the proposed formation mechanisms for nitrogen-containing products and multistep auto-oxidation products, starting from the BPR of $C_7H_9O_5$ (Sect. S1).
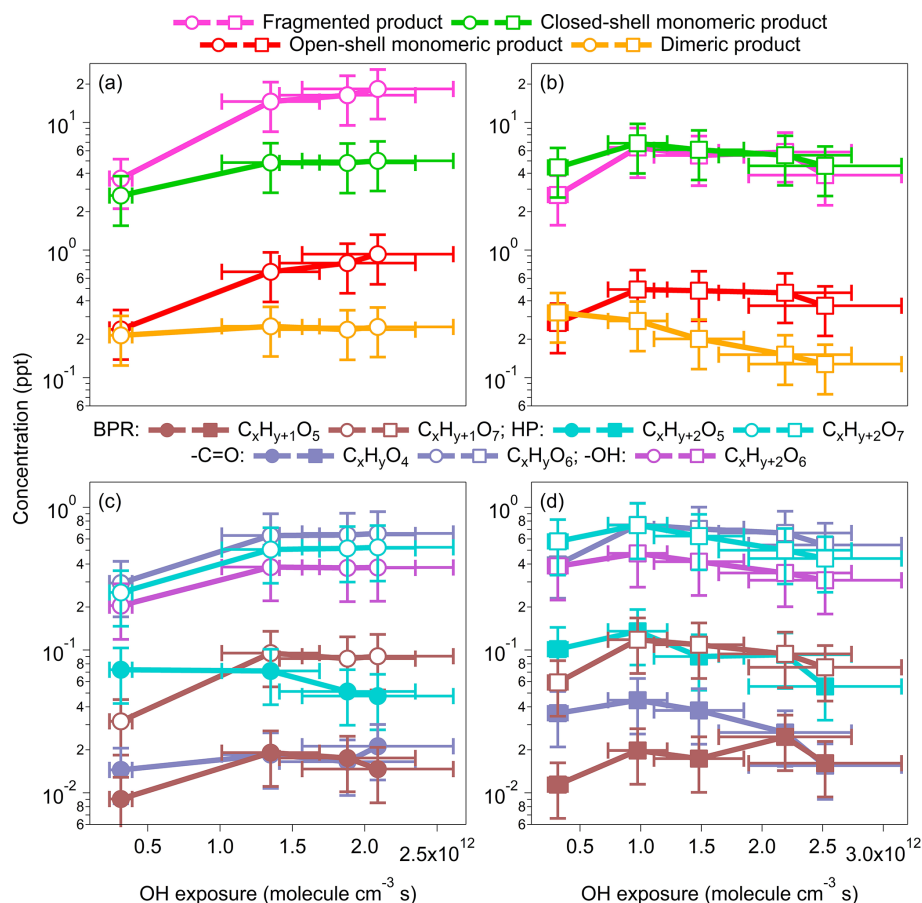
3.2 Low-NO_x conditions

Product distribution

The products that we observed herein (Tables S2–S3) are generally in agreement with those found in previous low-NO_x studies (Schwantes et al., 2017; Molteni et al., 2018; Zaytsev et al., 2019b; Mehra et al., 2020; Garmash et al., 2020). Differences exist in the relative abundance of species with different oxygen contents within each product category (Molteni et al., 2018; Garmash et al., 2020). Table S4 in the Supplement lists the experimental conditions and relative signal intensities of some major oxygenated products formed by benzene oxidation. Molteni et al. (2018) observes a predominant production of $C_6H_8O_5$ (plausibly hydroperoxides) and $C_{12}H_{14}O_8$. Garmash et al. (2020) shows relatively high signals of $C_6H_8O_9$ and $C_{12}H_{14}O_8$ in the flow tube experiments, whereas the chamber study and our study both show relatively high signals of $C_6H_8O_7$ and $C_6H_8O_9$ and lower signals of dimeric products. Moreover, the signal intensities of RO_2 (e.g., $C_6H_7O_5$ and $C_6H_7O_7$) are greater in our study than in other studies. Both experimental conditions and instrument detection are factors that may affect the product distribution. For example, a longer residence time might promote multistep auto-oxidation. For auto-oxidation, the H shift has rate constants of about 10^{-3} to $1\,s^{-1}$ and is likely the rate-determining step under atmospheric conditions, with reaction times of 1 to 10^3 s that are much longer than the subsequent O_2 addition of microseconds (hereafter µs) (Orlando et al., 2003; Bianchi et al., 2019). Garmash et al. (2020) indicated that fewer auto-oxidation steps would be expected in flow tube experiments. The flow tube study herein has a relatively longer residence time than others, which is consistent with relatively more abundant O_7 and O_9 products. Ambient environments have much lower OH concentrations but longer residence times, depending on meteorological conditions, which may suggest more oxygenated products from multisteps of auto-oxidation. Alternatively, the differences in HO_2 and RO_2 concentrations among different studies that remain unclear might affect the extent of auto-oxidation. For detection, the instrument efficiency might be different for HOMs with different clustering capabilities (e.g., numbers of functional groups as hydrogen bond donors; Hyttinen et al., 2015). Tuning might affect the transmission of product ions in different m/z ranges or affect the efficiency of dimer clustering (Heinritzi et al., 2016; Brophy and Farmer, 2015).

Effects of OH exposure

As shown in Fig. 2a, the concentrations of fragmented, monomeric closed-shell and open-shell and dimeric products formed by benzene oxidation increase with increasing OH exposure that corresponds to 2.4 to 16.1 d of atmospheric equivalent photochemical age. Elevated concentrations of monomeric open-shell products (e.g., RO_2) and HO_2 are ex-

Figure 2. Concentrations of fragmented, monomeric closed-shell, open-shell, and dimeric products formed by benzene and toluene oxidation under low-NO_x conditions (OFR254-5) at various OH exposures. For the benzene oxidation, both x and y are 6. For the toluene oxidation, x is 7, and y is 8. Note: BPR – bicyclic peroxy radical; HP – hydroperoxide; $-C=O$ – carbonyl; $-OH$ – alcohol.

pected for greater OH exposure, leading to enhanced production of the monomeric closed-shell and dimeric products through the $RO_2 + HO_2$ and $RO_2 + RO_2$ reactions. These processes may be limited by the availability of RO_2 (< 0.9 ppt (parts per trillion) in our study) rather than that of HO_2 (0.5–2.4 ppb; Table S1). Consistently, the concentrations of dimeric products are much lower than those of monomeric closed-shell products. For toluene oxidation, the dependence of the product formation on OH exposure is less significant than that for benzene (Fig. 2b). The concentrations of fragmented, monomeric closed-shell and open-shell products first increase and then slightly decrease with the increasing OH exposure that corresponds to 2.4 to 19.4 d of atmospheric equivalent photochemical age. Interestingly, unlike benzene oxidation, the concentrations of dimeric products decrease as the OH exposure increases, suggesting perhaps unfavorable dimer formation under conditions of high OH exposure for toluene oxidation. One potential contributor to the difference of the dependence of dimer formation on OH exposure is the more significant elevated RO_2 concentrations (0.2 to 0.9 ppt) as the OH exposure increases more for benzene oxidation

than that (0.3 to 0.5 ppt) for toluene oxidation, while the HO_2 concentrations in the two sets of experiments are similar (1.5–2.4 ppb). The enhancement of RO_2 concentrations may promote the dimer formation through the self- or cross-reactions of RO_2 (Mohr et al., 2017). On the other hand, a previous study indicates that the accretion of RO_2 depends on the functional groups of the RO_2 (Berndt et al., 2018). Whether the decreasing concentrations of dimeric products with OH exposure are related to the steric effects of the substituted methyl group of toluene requires further investigation. The overall atomic oxygen-to-carbon (O : C) ratios of HOM products increase from 1.18 to 1.26 for benzene oxidation and from 1.16 to 1.23 for toluene oxidation as the OH exposure increases, suggesting more oxygenated product distributions as detected. The overall atomic hydrogen-to-carbon (H : C) ratios of HOMs are 1.10–1.14 for benzene oxidation and 1.14–1.18 for toluene oxidation, and the changes with OH exposure are negligible.

Figure 2c–d show the concentrations of individual representative open-shell and closed-shell monomers for increasing OH exposures. The open-shell monomers are

mainly $C_xH_{y+1}O_5$ (BPRs) and $C_xH_{y+1}O_7$ (RO$_2$ formed from one more step of auto-oxidation). The concentrations of $C_xH_{y+1}O_7$ are approximately 1 order of magnitude higher than the concentrations of $C_xH_{y+1}O_5$. As described in Sect. 3.1, the further reactions of $C_xH_{y+1}O_5$ and $C_xH_{y+1}O_7$ may form closed-shell monomers, such as hydroperoxides ($C_xH_{y+2}O_{5,7}$), carbonyls ($C_xH_yO_{4,6}$), and alcohols ($C_xH_{y+2}O_{4,6}$; Mentel et al., 2015; Molteni et al., 2019), although these formulae may correspond to other functionalities, depending on the reaction rates and numbers of generation of autoxidation pathways. For multiple steps of auto-oxidation of BPRs or RO$_2$ radicals ($C_xH_{y+1}O_5$ or $C_xH_{y+1}O_7$), the products with two more hydrogen atoms than the precursor are plausibly hydroperoxides ($C_xH_{y+2}O_z$), if z is an odd number, and alcohols, if it is an even number. On the other hand, products that have the same hydrogen atoms ($C_xH_yO_z$) are likely carbonyls with an even number of z. Instead, if the carbonyl formation involves the RO pathway, $C_xH_yO_z$, with an odd number of z, may be formed. The concentrations of $C_xH_{y+2}O_7$ and $C_xH_yO_6$ originated from $C_xH_{y+1}O_7$ are 1 to 2 orders of magnitudes greater than the concentrations of $C_xH_{y+2}O_5$ and $C_xH_yO_4$, which originated from $C_xH_{y+1}O_5$. The greater signals of O$_7$ products suggest our experimental conditions perhaps favor the formation of more oxygenated products.

Enhanced formation of more oxygenated products was observed for elevated OH exposures. For example, the concentrations of $C_6H_7O_7$ increase first and stay relatively stable as the OH exposure increases, whereas the concentrations of $C_6H_7O_5$ decrease at high OH exposures for benzene oxidation. The concentrations of the hydroperoxide products ($C_xH_{y+2}O_{5,7}$), such as $C_6H_8O_7$, increase as OH exposure increases, whereas the concentrations of $C_6H_8O_5$ decreases. For toluene oxidation, the concentrations of $C_xH_{y+2}O_{5,7}$ ($C_7H_{10}O_5$ and $C_7H_{10}O_7$) both decrease. The concentrations of carbonyl products ($C_xH_yO_{4,6}$) increase with OH exposure for benzene but not for toluene. We do not observe significant signals for $C_xH_{y+2}O_4$ (alcohols) from BPR $C_xH_{y+1}O_5$, but $C_xH_{y+2}O_6$ from RO$_2$ $C_xH_{y+1}O_7$ are of high concentrations. The concentrations of $C_6H_8O_6$ (alcohol) from benzene also increase as the OH exposure increases, while the concentrations for $C_7H_{10}O_6$ from toluene decrease. Overall, the enhanced formation of more oxygenated products at high OH exposure is more significant for benzene than for toluene. A possible explanation is that toluene oxidation may involve more multigeneration OH oxidation because of the substituted methyl group.

Increasing OH exposure also enhances the formation of more oxygenated fragmented products (Fig. S6 in the Supplement). $C_4H_4O_3$ (perhaps epoxybutanedial) has been widely observed in aromatic oxidation (Wang et al., 2013; Wu et al., 2014; Zaytsev et al., 2019b). The concentrations of $C_4H_4O_3$ decrease monotonically as the OH exposure increases for both benzene and toluene oxidation. For toluene oxidation, $C_3H_4O_2$ (perhaps methylglyoxal), $C_4H_4O_2$ (per-

haps butenedial), and $C_5H_6O_2$ (perhaps methylbutenedial) that were detected by the PTR-QiTOF also show similar monotonic decreases. By contrast, the concentrations of $C_3H_4O_5$, $C_4H_4O_5$, and $C_5H_4O_6$ increase with increasing OH exposures for both benzene and toluene oxidation. The concentrations of other O$_{5-7}$ products also increase as the OH exposure increases. Similar to the monomeric open-shell and closed-shell products, the increasing trends are more significant for benzene-derived products than those for toluene-derived ones. This observation is in agreement with Garmash et al. (2020), who suggested that first-generation fragmented products were converted to more oxygenated ones through further oxidation as the OH exposure increases. Alternatively, these more oxygenated fragmented products might also be direct decomposition products of highly oxygenated RO radicals, which have been shown to play important roles in product formation (Noda et al., 2009; Birdsall and Elrod, 2011).

Multigeneration OH oxidation

In benzene and toluene (C_xH_y) oxidation by OH radicals, we may expect that one OH addition could lead to termination products with hydrogen numbers of y and $y + 2$. When the second OH attack occurs, products with hydrogen numbers $< y$ and $> y + 2$ may be produced by multigeneration OH reactions (Table S5 in the Supplement). For example, the closed-shell monomeric products from benzene oxidation should contain at least one double bond which can further react with OH radicals via OH addition to form products with two more hydrogen atoms (e.g., to form $C_6H_{10}O_z$). The formation of $C_6H_4O_z$ from the closed-shell monomeric products of benzene oxidation may involve multigeneration OH reactions via H abstraction and subsequent termination by a loss of OH or HO$_2$ (Molteni et al., 2018; Garmash et al., 2020). There are significant contributions of products with hydrogen numbers $< y$ and $> y + 2$ in our experiments (Tables S2 and S3), highlighting the importance of multigeneration OH reactions in production formation. On the other hand, the formation of y and $y + 2$ products may also involve multistep OH addition or H subtraction that make conversions between the two groups of products. For the phenolic pathway, the main products of $C_6H_6O_z$ and $C_7H_8O_z$ may be produced by dihydroxy-OH, trihydroxy-OH, and even multi-OH substituted benzene or toluene (Schwantes et al., 2017). The contributions of a third of the OH attack on the total of detected signals are often very low (Molteni et al., 2018).

Figure 3 shows the concentrations and the relative contributions of the closed-shell monomeric product groups, including $C_xH_{y-2}O_z$, $C_xH_yO_z$, $C_xH_{y+2}O_z$, and $C_xH_{y+4}O_z$. For both benzene and toluene oxidation, the concentrations of these monomers increase as the OH exposure increases for the atmospherically relevant equivalent photochemical age (< 10 d). For greater OH exposures, the concentrations of $y - 2$ products keep increasing, whereas the concentrations of
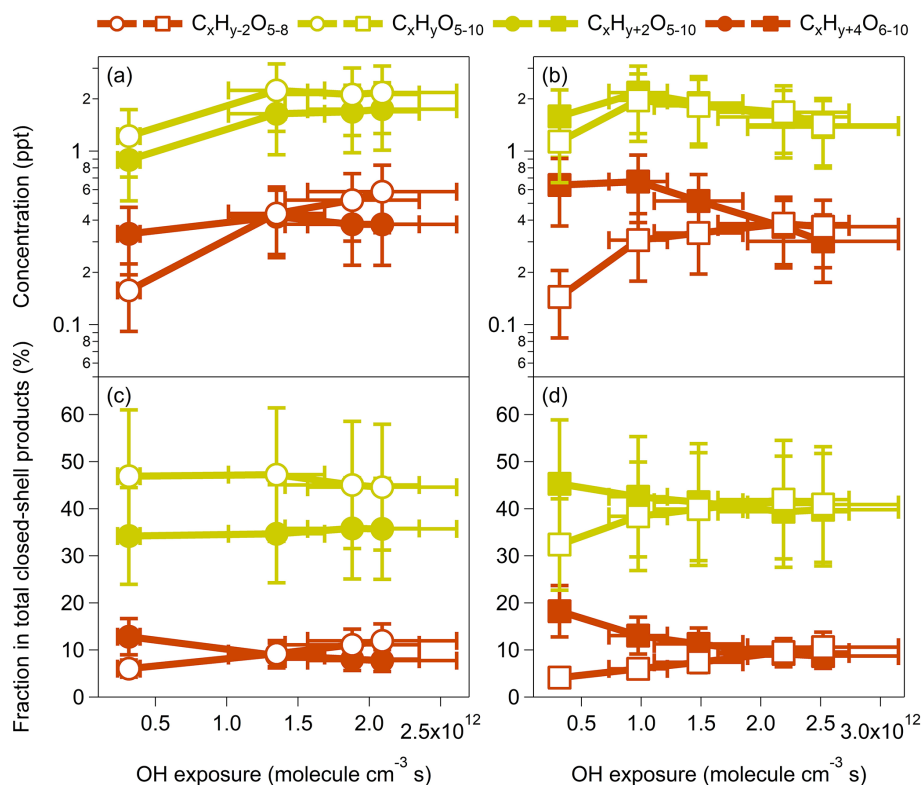
Figure 3. Concentrations and relative contributions of closed-shell monomeric products formed by benzene and toluene oxidation under low-NO$_x$ conditions (OFR254-5) at various OH exposures. For the benzene oxidation, both x and y are 6. For the toluene oxidation, x is 7, and y is 8.

other products start to decrease (Fig. 3a–b). The decreasing trends at high OH exposures are more significant for toluene-derived products. Such differences might be explained by (1) the faster OH + VOC rate for toluene than for benzene and (2) the methyl group in toluene and the added −OH groups during oxidation that may increase the electron density on the aromatic ring through a resonant electron-donating effect and, thereby, activate the aromatic ring and facilitate further addition reactions to form products with multiple −OH groups (M. Wang et al., 2020). Interestingly, the relative fractions of the C$_x$H$_{y-2}$O$_z$ and C$_x$H$_{y+4}$O$_z$ products for both benzene and toluene oxidation show opposite trends (Fig. 3c–d). The increasing fractions of y-2 products but decreasing fractions of $y + 4$ products for increasing OH exposures, as well as the monotonically increasing concentration of y-2 products, suggest that the multigeneration OH oxidation may proceed preferably via H subtraction rather than OH addition, according to the current mechanistic understanding of aromatic oxidation. Garmash et al. (2020) also noted that higher OH concentrations caused a larger variety in HOM products, with H abstraction oxidation becoming possibly more significant. Compared with their precursors (benzene and toluene), the closed-shell monomeric products are less conjugated, and thus, OH addition is probably less favorable.

Estimated molar yields

Figure S7 in the Supplement shows the scatterplot of the concentrations of HOMs detected by NO$_3^-$-TOF-CIMS and the VOC oxidation rate for benzene and toluene oxidation under low-NO$_x$ conditions. As expected, the product concentrations increase with the VOC oxidation rates. To calculate the molar yields of HOM products, wall losses are corrected, including the loss in the sampling line, the loss to the OFR walls estimated by eddy diffusion, the loss to aerosol particles in the OFR (i.e., the condensation sink calculated on the basis of particle measurements), and the loss to non-condensable products due to continuous reaction with OH (Palm et al., 2016). Details are provided in Sect. S4 in the Supplement. Our estimated molar yields for the HOM products are 0.22 ± 0.10 % (mean $\pm$ 1 standard deviation) for benzene oxidation and 0.46 ± 0.20 % for toluene oxidation. These yields are much lower than the smog chamber results of 4.1 % to 14.0 % for benzene oxidation reported by Garmash et al. (2020) but slightly greater than the flow tube yields of 0.1 % to 0.2 % reported by Molteni et al. (2018). A key difference in the experimental conditions is the much longer residence time in the chamber study (Table S4), suggesting, perhaps, a long characteristic time of HOM formation from aromatic oxidation. The study of
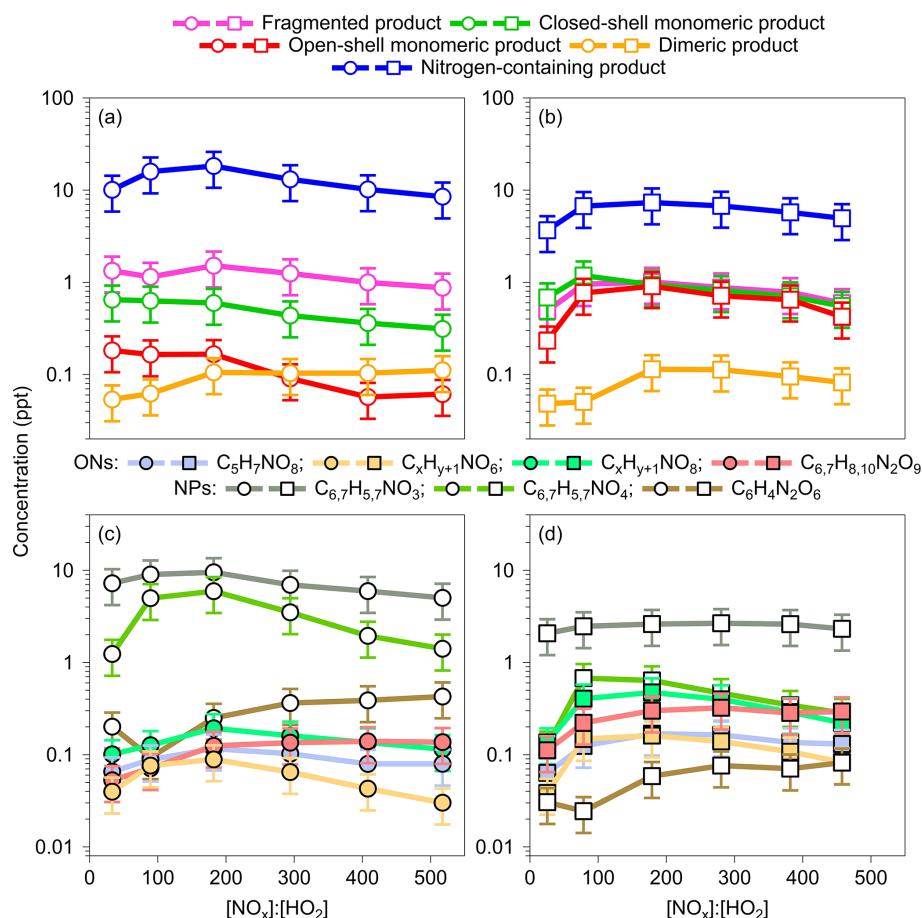
Figure 4. Concentrations of fragmented, monomeric closed-shell, open-shell, dimeric, and nitrogen-containing products formed by benzene and toluene oxidation under high-NO_x conditions (OFR254-5–$iN_2O1.1/4.4$) at various $[NO_x]:[HO_2]$ levels. Data for OFR254-5–$iN_2O1.1$ experiments were averaged and are shown as the first data point in each panel. For the benzene oxidation, both x and y are 6. For the toluene oxidation, x is 7, and y is 8.

Molteni et al. (2018) only provided the initial OH concentration (as listed in Table S4) that should decrease significantly as the reaction proceeded, for which we cannot rule out the possibility of low OH exposure that leads to fewer oxidation steps (i.e., lower yields of HOMs). Instrument sensitivity might also affect the detection of HOMs but is less likely to lead to orders of magnitude difference in the yields.

3.3 High-NO_x conditions

Effects of NO_x level

The NO or NO_2 termination of RO_2 radicals competes with the HO_2 or RO_2 termination and forms nitrogen-containing species at the expense of other highly oxygenated products (Tsiligiannis et al., 2019; Garmash et al., 2020; Y. Wang et al., 2020; Mehra et al., 2020). Yet, quantitative understanding in the effects of NO_x on the formation of oxygenated products is limited for aromatic precursors compared with those for biogenic VOCs (Nah et al., 2016; Lambe

et al., 2017; Sarnela et al., 2018). The high-NO_x experiments herein were conducted with $[NO_2]:[NO]$ ratios of 20 to 120 (Table S1), which may represent urban afternoon conditions when fresh NO_x emission is mostly converted to NO_2, and intense photochemistry fuels the oxidation of aromatics accompanying the NO_x emission (Newland et al., 2021). Figure 4 shows the concentrations of observed HOMs for various $[NO_x]:[HO_2]$ conditions. We use $[NO_x]:[HO_2]$ instead of $[NO]:[HO_2]$ to evaluate termination pathways to form various nitrogen-containing products such as nitrated phenols, organic nitrate, and peroxynitrate. The contributions from $RO_2 + RO_2$ termination are probably minor because of the low concentrations of RO_2 (< 0.9 ppt). Given the low and narrow range of NO_x levels in the OFR254–$iN_2O1.1$ experiments, the product concentrations for all lamp voltages (i.e., a range of OH exposure) are averaged and shown as the first data point in each panel of Fig. 4.

Similar to previous findings, nitrogen-containing products are the dominant species in the spectra, with concentrations up to 18.3 and 7.3 ppt for benzene and toluene oxidation, re-
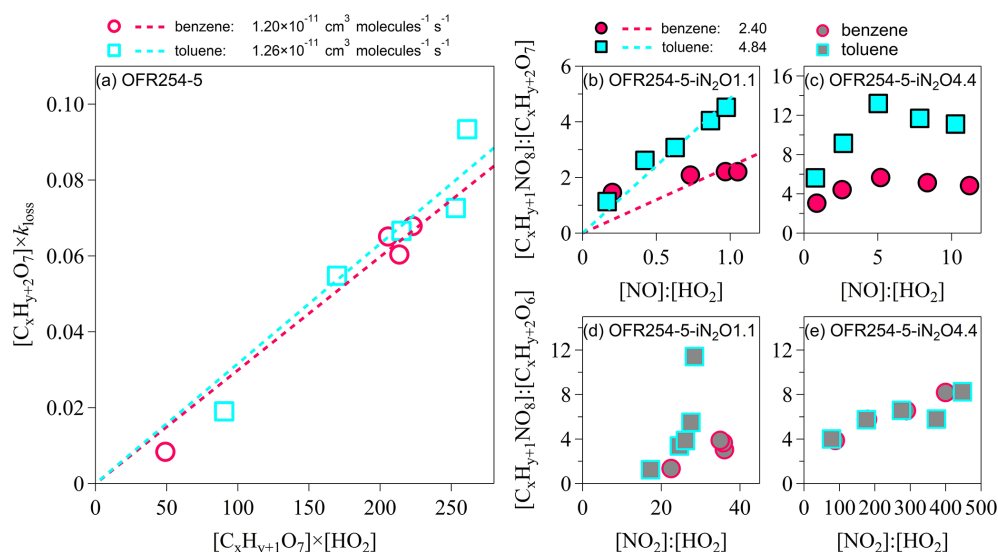
Figure 5. Kinetic analysis on the formation of nitrogen-containing HOMs. **(a)** $[ROOH] \times k_{loss}$ vs. $[RO_2][HO_2]$. **(b–c)** $[RONO_2] : [ROOH]$ vs. $[NO] : [HO_2]$. **(d–e)** $[RC(O)OONO_2] : [ROOH]$ vs. $[NO_2] : [HO_2]$. For the benzene oxidation, both x and y are 6. For the toluene oxidation, x is 7, and y is 8. k_{loss} represents the loss rate of the corresponding HOM products in units per second (hereafter s^{-1}).

spectively. The concentrations of all HOMs start to decrease at high $[NO_x] : [HO_2]$ ratios, except that the concentrations of dimeric products from benzene oxidation remain steady (Fig. 4a–b). The decreasing trends for monomeric closed-shell, open-shell, and fragmented products are expected, indicating significant competition of radical terminations by NO or NO_2. The decreasing concentrations of nitrogen-containing products for increasing $[NO_x] : [HO_2]$ are, however, counterintuitive. Figure 4c–d show the concentrations of main individual nitrogen-containing products. The initial increase in the concentrations of nitrogen-containing species might be explained by a decrease in HO_2 concentrations from 0.8–1.5 to 0.5–0.7 ppb as a result of the switch of 1.1 % of N_2O injection to 4.4 % (Table S1). The further reduction in these compounds as $[NO_x] : [HO_2]$ increases is probably related to the simultaneous decrease in RO_2 or, alternatively, further reactions to products that have two nitrogen atoms. Figure S8 in the Supplement shows similar concentration trends for individual ring scission and ring-retaining products with or without nitrogen in their formulas. There seem to be optimal $[NO_x] : [HO_2]$ ratios of 130 to 240 for the formation of nitrogen-containing products. The dependence of those products with only one nitrogen atom on NO_x is, however, not strong. The availability of RO_2 is perhaps the key factor that limits their formation at low NO_x levels and affects further reactions to form products with two nitrogen atoms at high NO_x levels.

Nitrated phenols are the most abundant nitrogen-containing products under high-NO_x conditions. In aromatic oxidation, these compounds are formed by the reaction of phenoxy RO radicals with NO_2 (Jenkin et al., 2003). In the Master Chemical Mechanism (MCMv3.3.1), the phe-

noxy RO radicals can be formed via OH oxidation of phenols ($k_{OH} = 2.8 \times 10^{-11}$ cm^3 mol^{-1} s^{-1}), with a low branching ratio of 0.06. They can also be formed by the NO_3 oxidation of phenols ($k_{NO_3} = 3.8 \times 10^{-12}$ cm^3 mol^{-1} s^{-1}), with a high branching ratio of 0.74 (IUPAC, 2008). Under high-NO_x conditions, the estimated concentrations of OH and NO_3 radicals are 0.05 to 0.3 ppb and 0.01 to 0.09 ppb, respectively, suggesting that the NO_3 oxidation of phenols contributed efficiently to the formation of nitrated phenols in the OFR experiments herein. When $[NO_x] : [HO_2]$ increases, the concentrations of $C_{6,7}H_{5,7}NO_4$ (perhaps nitrocatechol or methylnitrocatechol) increase first and then decrease. The concentrations of $C_{6,7}H_{5,7}NO_3$ (perhaps nitrophenol or methylnitrophenol), however, show a weak dependence on the NO_x level, suggesting the availability of RO radical might be the limiting factor in controlling the formation of nitrated phenols herein. Interestingly, the concentrations of products with two nitrogen atoms such as $C_6H_4N_2O_6$, $C_6H_8N_2O_9$, and $C_7H_{10}N_2O_9$ (only for toluene) steadily increase as $[NO_x] : [HO_2]$ rises, suggesting a strong dependence of the formation of these species on NO_2.

Formation of ROOH, RONO₂, and ROONO₂

Jenkin et al. (2019) suggested that the overall rate coefficients for $RO_2 + HO_2$ reactions are 1.92×10^{-11} and 1.98×10^{-11} cm^3 mol^{-1} s^{-1} at 298 K for benzene and toluene oxidation, respectively. For the OFR conditions (Table S1), the characteristic time for the RO_2 termination by HO_2 was perhaps < 10 s, which is much shorter than the OFR residence time of 95 s. The rate coefficients of the hydroperoxide pathway ($RO_2 + HO_2 \rightarrow ROOH + O_2$) may be con-

strained by the concentration ratios of [ROOH] multiplied by the loss rate of ROOH to [RO$_2$][HO$_2$] (Sect. S5 in the Supplement). For example, assuming that the C$_6$H$_7$O$_7$ and C$_7$H$_9$O$_7$ are the RO$_2$ radicals, and C$_6$H$_8$O$_7$ and C$_7$H$_{10}$O$_7$ are the corresponding ROOH for benzene and toluene oxidation, respectively, the slopes in Fig. 5a indicate that the rate coefficients of hydroperoxides are 1.20×10^{-11} and 1.26×10^{-11} cm^3 mol^{-1} s^{-1}. These rate coefficients suggest that the branching ratios of the hydroperoxide formation under low-NO$_x$ conditions are 0.62 and 0.64 for benzene- and toluene-derived RO$_2$, respectively, which are consistent with the estimated branching ratios of 0.52–1.00 in the literature (Jenkin et al., 2019).

In the presence of NO$_x$, the reactions between C$_x$H$_{y+1}$O$_7$ and nitrogen oxides lead to both chain propagation and chain termination to form RO radicals and nitrogen-containing products. Similar to the analysis of the hydroperoxide formation, the slopes in Fig. 5b suggest that the rate coefficients of RO$_2$+NO(+M) → RONO$_2$(+M) are 2.87×10^{-11} and 6.12×10^{-11} cm^3 mol^{-1} s^{-1} for benzene and toluene oxidation under OFR254-5–iN$_2$O1.1 conditions, respectively (Sect. S5). These coefficients are more than 1 order of magnitude greater than the values reported by Jenkin et al. (2019; i.e., 8.09×10^{-13} and 1.10–8.45×10^{-13} cm^3 mol^{-1} s^{-1} for benzene and toluene oxidation, respectively). One explanation is that the detected C$_x$H$_{y+1}$NO$_8$ contains multifunctional groups and represents not only non-peroxy organic nitrates (RONO$_2$) but also peroxy organic nitrates (ROONO$_2$). As shown in Fig. 5c, the [C$_x$H$_{y+1}$NO$_8$] : [C$_x$H$_{y+2}$O$_7$] ratios start to decrease at higher [NO] : [HO$_2$] in our OFR254-5—iN$_2$O4.4 experiments. The competition between NO and HO$_2$ for terminating RO$_2$ should not alter the rate coefficients and the branching ratios (Atkinson and Arey, 2003). The lack of a linear relationship of [C$_x$H$_{y+1}$NO$_8$] : [C$_x$H$_{y+2}$O$_7$] (i.e., assumed as [RONO$_2$] : [ROOH]) on [NO] : [HO$_2$] ratio is consistent, with the possibility of C$_x$H$_{y+1}$O$_8$ partially being ROONO$_2$, especially for toluene oxidation.

Xu et al. (2020) indicate that the formation of non-peroxy organic nitrates (RONO$_2$) is minor in aromatic oxidation. The detected ROONO$_2$ are likely RC(O)OONO$_2$ because ROONO$_2$ are usually thermally unstable intermediates (Kirchner et al., 1999), and RC(O)OONO$_2$ can be detected by the NO$_3^-$-TOF-CIMS (Rissanen, 2018). Acyl peroxy radicals RC(O)OO (i.e., a type of peroxy radical) may react with NO$_2$ to produce peroxyacyl nitrate (RC(O)OONO$_2$; Jenkin et al., 2019). The formation of the RC(O)OONO$_2$ requires (1) the original RO$_2$ radicals to be C$_x$H$_{y+1}$O$_6$ instead of C$_x$H$_{y+1}$O$_7$, and (2) an acyl (−C=O) group that is connected to the O−O bond. The formation of C$_x$H$_{y+1}$O$_6$ is feasible through the RO pathway (Sect. S3). The hydroperoxides corresponding to C$_x$H$_{y+1}$O$_6$ are C$_x$H$_{y+2}$O$_6$ (i.e., C$_6$H$_8$O$_6$ and C$_7$H$_{10}$O$_6$ for benzene and toluene, respectively). Figure 5d–e show the increase in [C$_x$H$_{y+1}$NO$_8$] : [C$_x$H$_{y+2}$O$_6$] (i.e., perhaps [RC(O)OONO$_2$] : [ROOH]) for increasing [NO$_2$] : [HO$_2$] ratios. In particular, the relationship be-

tween [C$_x$H$_{y+1}$NO$_8$] : [C$_x$H$_{y+2}$O$_6$] and [NO$_2$] : [HO$_2$] is nearly linear at high [NO$_2$] : [HO$_2$] ratios in the OFR254-5–iN$_2$O4.4 experiments. There is a lack of kinetic data for the reactions of RC(O)OO + NO$_2$ (Rissanen, 2018), which prevents us from further investigation.

4 Atmospheric implications

In this study, we investigated the formation of HOMs in the OFR by the oxidation of benzene and toluene in a wide range of OH exposure and NO$_x$ conditions. Recent findings emphasize the significance of the bicyclic channel in the oxidation of light aromatics (Wang et al., 2017; Molteni et al., 2018; Tsiligiannis et al., 2019; Zaytsev et al., 2019b; Garmash et al., 2020; Y. Wang et al., 2020). The presence of NO$_x$ enhances the formation of organonitrates and even dinitrate organic compounds. Extensive autoxidation and accretion reaction has been reported for substituted aromatics (Y. Wang et al., 2020). Our results show enhanced formation of more oxygenated products for elevated OH exposures. The formation of dimeric products, however, seems unfavorable under conditions of high OH exposure and low NO$_x$ for substituted aromatics. The suppression of dimeric products may affect the contribution of aromatic HOMs to new particle formation in the downwind of urban atmosphere. The changes in product distribution and concentration highlight the possibility that multigeneration OH oxidation proceed preferably via H subtraction rather than OH addition, although one HOM formula may correspond to various functionalities. For aged air masses, this may reduce the H : C ratios of HOM products from aromatic oxidation. Under high-NO$_x$ conditions, we show that the formation of products containing one nitrogen atom perhaps depends more significantly on the organic radicals (RO or RO$_2$) but less so on NO$_2$, while the formation of products containing two nitrogen atoms depends significantly on NO$_2$. Further investigation on the roles of high-NO$_2$ conditions that represent a wide range of anthropogenically influenced environments in the oxidation of aromatic VOCs are needed. Moreover, we found that non-peroxy organic nitrates might form via RO$_2$ + NO under low-NO$_2$ conditions, and RO$_2$ + NO$_2$ may dominate to produce ROONO$_2$ or RC(O)OONO$_2$ under high-NO$_2$ conditions. The reaction of RC(O)OO with NO$_2$ to produce peroxyacyl nitrates should be of particular importance with high [NO$_2$] : [NO] ratios of tens to hundreds. Both of ROONO$_2$ and RC(O)OONO$_2$ are reservoirs of RO$_2$ radicals. Under conditions of high [NO$_2$] : [NO] ratios (e.g., late afternoon in urban or suburban environments), the effective lifetimes of RO$_2$ radicals might become longer because of the formation of RC(O)OONO$_2$. Subsequent slow release of RO$_2$ radicals with the help of NO$_2$ may extend the formation of HOMs from VOC oxidation in urban environments to early evening, when OH starts to decline and NO$_3$ has not yet built up, facilitating the development of regional SOA pollution.

References

Arey, J., Obermeyer, G., Aschmann, S. M., Chattopadhyay, S., Cusick, R. D., and Atkinson, R.: Dicarbonyl products of the OH radical-initiated reaction of a series of aromatic hydrocarbons, Environ. Sci. Technol., 43, 683–689, https://doi.org/10.1021/es8019098, 2009.

Atkinson, R.: Atmospheric chemistry of VOCs and NO_x, Atmos. Environ., 34, 2063–2101, https://doi.org/10.1016/S1352-2310(99)00460-4, 2000.

Atkinson, R. and Arey, J.: Atmospheric degradation of volatile organic compounds, Chem. Rev., 103, 4605–4638, https://doi.org/10.1021/cr0206420, 2003.

Berndt, T., Richters, S., Jokinen, T., Hyttinen, N., Kurten, T., Otkjaer, R. V., Kjaergaard, H. G., Stratmann, F., Herrmann, H., Sipila, M., Kulmala, M., and Ehn, M.: Hydroxyl radical-induced formation of highly oxidized organic compounds, Nat. Commun., 7, 13677, https://doi.org/10.1038/ncomms13677, 2016.

Berndt, T., Scholz, W., Mentler, B., Fischer, L., Herrmann, H., Kulmala, M., and Hansel, A.: Accretion product formation from self- and cross-reactions of RO2 radicals in the atmosphere, Angew. Chem.-Ger. Edit., 57, 3820–3824, https://doi.org/10.1002/anie.201710989, 2018.

Bianchi, F., Kurten, T., Riva, M., Mohr, C., Rissanen, M. P., Roldin, P., Berndt, T., Crounse, J. D., Wennberg, P. O., Mentel, T. F., Wildt, J., Junninen, H., Jokinen, T., Kulmala, M., Worsnop, D. R., Thornton, J. A., Donahue, N., Kjaergaard, H. G., and Ehn, M.: Highly oxygenated organic molecules (HOM) from gas-phase autoxidation involving peroxy radicals: a key contributor to atmospheric aerosol, Chem. Rev., 119, 3472–3509, https://doi.org/10.1021/acs.chemrev.8b00395, 2019.

Birdsall, A. W. and Elrod, M. J.: Comprehensive NO-dependent study of the products of the oxidation of atmospherically relevant aromatic compounds, J. Phys. Chem. A, 115, 5397–5407, https://doi.org/10.1021/jp2010327, 2011.

Birdsall, A. W., Andreoni, J. F., and Elrod, M. J.: Investigation of the role of bicyclic peroxy radicals in the oxidation mechanism of toluene, J. Phys. Chem. A, 114, 10655–10663, https://doi.org/10.1021/jp105467e, 2010.

Brophy, P. and Farmer, D. K.: A switchable reagent ion high resolution time-of-flight chemical ionization mass spectrometer for real-time measurement of gas phase oxidized species: characterization from the 2013 southern oxidant and aerosol study, Atmos. Meas. Tech., 8, 2945–2959, https://doi.org/10.5194/amt-8-2945-2015, 2015.

Calvert, J. G., Atkinson, R., Becker, K. H., Kamens, R. M., Seinfeld, J. H., Wallington, T. J., and Yarwood, G. Y.: The mechanisms of atmospheric oxidation of aromatic hydrocarbons, Oxford University Press, New York, 2002.

Calvert, J. G., Orlando, J. J., Stockwell, W. R., and Wallington, T. J.: The mechanisms of reactions influencing atmospheric ozone, Oxford University Press, New York, 2015.

Cheng, X., Chen, Q., Li, Y., Huang, G., Liu, Y., Lu, S., Zheng, Y., Qiu, W., Lu, K., Qiu, X., Bianchi, F., Yan, C., Yuan, B., Shao, M., Wang, Z., Canagaratna, M. R., Zhu, T., Wu, Y., and Zeng, L.: Secondary Production of Gaseous Nitrated Phenols in Polluted Urban Environments, Environ. Sci. Technol., 55, 4410–4419, https://doi.org/10.1021/acs.est.0c07988, 2021.

Crounse, J. D., Nielsen, L. B., Jørgensen, S., Kjaergaard, H. G., and Wennberg, P. O.: Autoxidation of organic compounds in the atmosphere, J. Phys. Chem. Lett., 4, 3513–3520, https://doi.org/10.1021/jz4019207, 2013.

Ehn, M., Thornton, J. A., Kleist, E., Sipila, M., Junninen, H., Pullinen, I., Springer, M., Rubach, F., Tillmann, R., Lee, B., Lopez-Hilfiker, F., Andres, S., Acir, I. H., Rissanen, M., Jokinen, T., Schobesberger, S., Kangasluoma, J., Kontkanen, J., Nieminen, T., Kurten, T., Nielsen, L. B., Jorgensen, S., Kjaergaard, H. G., Canagaratna, M., Dal Maso, M., Berndt, T., Petaja, T., Wahner, A., Kerminen, V. M., Kulmala, M.,

Worsnop, D. R., Wildt, J., and Mentel, T. F.: A large source of low-volatility secondary organic aerosol, Nature, 506, 476–479, https://doi.org/10.1038/nature13032, 2014.

Gallimore, P. J., Achakulwisut, P., Pope, F. D., Davies, J. F., Spring, D. R., and Kalberer, M.: Importance of relative humidity in the oxidative ageing of organic aerosols: case study of the ozonolysis of maleic acid aerosol, Atmos. Chem. Phys., 11, 12181–12195, https://doi.org/10.5194/acp-11-12181-2011, 2011.

Garmash, O., Rissanen, M. P., Pullinen, I., Schmitt, S., Kausiala, O., Tillmann, R., Zhao, D., Percival, C., Bannan, T. J., Priestley, M., Hallquist, Å. M., Kleist, E., Kiendler-Scharr, A., Hallquist, M., Berndt, T., McFiggans, G., Wildt, J., Mentel, T. F., and Ehn, M.: Multi-generation OH oxidation as a source for highly oxygenated organic molecules from aromatics, Atmos. Chem. Phys., 20, 515–537, https://doi.org/10.5194/acp-20-515-2020, 2020.

Gowda, D. and Kawamura, K.: Seasonal variations of low molecular weight hydroxy-dicarboxylic acids and oxaloacetic acid in remote marine aerosols from Chichijima Island in the western North Pacific (December 2010–November 2011), Atmos. Res., 204, 128–135, https://doi.org/10.1016/j.atmosres.2018.01.007, 2018.

Heinritzi, M., Simon, M., Steiner, G., Wagner, A. C., Kürten, A., Hansel, A., and Curtius, J.: Characterization of the mass-dependent transmission efficiency of a CIMS, Atmos. Meas. Tech., 9, 1449–1460, https://doi.org/10.5194/amt-9-1449-2016, 2016.

Huang, G., Liu, Y., Shao, M., Li, Y., Chen, Q., Zheng, Y., Wu, Z., Liu, Y., Wu, Y., Hu, M., Li, X., Lu, S., Wang, C., Liu, J., Zheng, M., and Zhu, T.: Potentially important contribution of gas-phase oxidation of naphthalene and methylnaphthalene to secondary organic aerosol during haze events in Beijing, Environ. Sci. Technol., 53, 1235–1244, https://doi.org/10.1021/acs.est.8b04523, 2019.

Hyttinen, N., Kupiainen-Määttä, O., Rissanen, M. P., Muuronen, M., Ehn, M., and Kurtén, T.: Modeling the charging of highly oxidized cyclohexene ozonolysis products using nitrate-based chemical ionization, J. Phys. Chem. A, 119, 6339–6345, https://doi.org/10.1021/acs.jpca.5b01818, 2015.

IUPAC: available at: http://iupac.pole-ether.fr (last access: 24 July 2021), 2008.

Jenkin, M. E., Saunders, S. M., Wagner, V., and Pilling, M. J.: Protocol for the development of the Master Chemical Mechanism, MCM v3 (Part B): tropospheric degradation of aromatic volatile organic compounds, Atmos. Chem. Phys., 3, 181–193, https://doi.org/10.5194/acp-3-181-2003, 2003.

Jenkin, M. E., Valorso, R., Aumont, B., and Rickard, A. R.: Estimation of rate coefficients and branching ratios for reactions of organic peroxy radicals for use in automated mechanism construction, Atmos. Chem. Phys., 19, 7691–7717, https://doi.org/10.5194/acp-19-7691-2019, 2019.

Jokinen, T., Sipilä, M., Junninen, H., Ehn, M., Lönn, G., Hakala, J., Petäjä, T., Mauldin III, R. L., Kulmala, M., and Worsnop, D. R.: Atmospheric sulphuric acid and neutral cluster measurements using CI-APi-TOF, Atmos. Chem. Phys., 12, 4117–4125, https://doi.org/10.5194/acp-12-4117-2012, 2012.

Kirchner, F., Mayer-Figge, A., Zabel, F., and Becker, K. H.: Thermal stability of peroxynitrates, Int. J. Chem. Kinet., 31, 127–144, https://doi.org/10.1002/(sici)1097-4601(1999)31:2<127::aid-kin6>3.0.co;2-l, 1999.

Lambe, A., Massoli, P., Zhang, X., Canagaratna, M., Nowak, J., Daube, C., Yan, C., Nie, W., Onasch, T., Jayne, J., Kolb, C., Davidovits, P., Worsnop, D., and Brune, W.: Controlled nitric oxide production via O(^{1}D) + N$_2$O reactions for use in oxidation flow reactor studies, Atmos. Meas. Tech., 10, 2283–2298, https://doi.org/10.5194/amt-10-2283-2017, 2017.

Lambe, A. T., Ahern, A. T., Williams, L. R., Slowik, J. G., Wong, J. P. S., Abbatt, J. P. D., Brune, W. H., Ng, N. L., Wright, J. P., Croasdale, D. R., Worsnop, D. R., Davidovits, P., and Onasch, T. B.: Characterization of aerosol photooxidation flow reactors: heterogeneous oxidation, secondary organic aerosol formation and cloud condensation nuclei activity measurements, Atmos. Meas. Tech., 4, 445–461, https://doi.org/10.5194/amt-4-445-2011, 2011.

Li, L., Tang, P., Nakao, S., and Cocker III, D. R.: Impact of molecular structure on secondary organic aerosol formation from aromatic hydrocarbon photooxidation under low-NO$_x$ conditions, Atmos. Chem. Phys., 16, 10793–10808, https://doi.org/10.5194/acp-16-10793-2016, 2016.

Mehra, A., Wang, Y., Krechmer, J. E., Lambe, A., Majluf, F., Morris, M. A., Priestley, M., Bannan, T. J., Bryant, D. J., Pereira, K. L., Hamilton, J. F., Rickard, A. R., Newland, M. J., Stark, H., Croteau, P., Jayne, J. T., Worsnop, D. R., Canagaratna, M. R., Wang, L., and Coe, H.: Evaluation of the chemical composition of gas- and particle-phase products of aromatic oxidation, Atmos. Chem. Phys., 20, 9783–9803, https://doi.org/10.5194/acp-20-9783-2020, 2020.

Mentel, T. F., Springer, M., Ehn, M., Kleist, E., Pullinen, I., Kurtén, T., Rissanen, M., Wahner, A., and Wildt, J.: Formation of highly oxidized multifunctional compounds: autoxidation of peroxy radicals formed in the ozonolysis of alkenes – deduced from structure–product relationships, Atmos. Chem. Phys., 15, 6745–6765, https://doi.org/10.5194/acp-15-6745-2015, 2015.

Mohr, C., Lopez-Hilfiker, F. D., Yli-Juuti, T., Heitto, A., Lutz, A., Hallquist, M., D'Ambro, E. L., Rissanen, M. P., Hao, L., Schobesberger, S., Kulmala, M., Mauldin III, R. L., Makkonen, U., Sipilä, M., Petäjä, T., and Thornton, J. A.: Ambient observations of dimers from terpene oxidation in the gas phase: Implications for new particle formation and growth, Geophys. Res. Lett., 44, 2958–2966, https://doi.org/10.1002/2017gl072718, 2017.

Molteni, U., Bianchi, F., Klein, F., El Haddad, I., Frege, C., Rossi, M. J., Dommen, J., and Baltensperger, U.: Formation of highly oxygenated organic molecules from aromatic compounds, Atmos. Chem. Phys., 18, 1909–1921, https://doi.org/10.5194/acp-18-1909-2018, 2018.

Molteni, U., Simon, M., Heinritzi, M., Hoyle, C. R., Bernhammer, A.-K., Bianchi, F., Breitenlechner, M., Brilke, S., Dias, A., Duplissy, J., Frege, C., Gordon, H., Heyn, C., Jokinen, T., Kuerten, A., Lehtipalo, K., Makhmutov, V., Petaja, T., Pieber, S. M., Praplan, A. P., Schobesberger, S., Steiner, G., Stozhkov, Y., Tome, A., Trostl, J., Wagner, A. C., Wagner, R., Williamson, C., Yan, C., Baltensperger, U., Curtius, J., Donahue, N. M., Hansel, A., Kirkby, J., Kulmala, M., Worsnop, D. R., and Dommen, J.: Formation of highly oxygenated organic molecules from α-pinene ozonolysis: chemical characteristics, mechanism, and kinetic model development, ACS Earth Space Chem., 3, 873–883, https://doi.org/10.1021/acsearthspacechem.9b00035, 2019.

Nah, T., Sanchez, J., Boyd, C. M., and Ng, N. L.: Photochemical aging of α-pinene and β-pinene secondary organic aerosol formed from nitrate radical oxidation, Environ. Sci. Technol., 50, 222–231, https://doi.org/10.1021/acs.est.5b04594, 2016.

Newland, M. J., Bryant, D. J., Dunmore, R. E., Bannan, T. J., Acton, W. J. F., Langford, B., Hopkins, J. R., Squires, F. A., Dixon, W., Drysdale, W. S., Ivatt, P. D., Evans, M. J., Edwards, P. M., Whalley, L. K., Heard, D. E., Slater, E. J., Woodward-Massey, R., Ye, C., Mehra, A., Worrall, S. D., Bacak, A., Coe, H., Percival, C. J., Hewitt, C. N., Lee, J. D., Cui, T., Surratt, J. D., Wang, X., Lewis, A. C., Rickard, A. R., and Hamilton, J. F.: Low-NO atmospheric oxidation pathways in a polluted megacity, Atmos. Chem. Phys., 21, 1613–1625, https://doi.org/10.5194/acp-21-1613-2021, 2021.

Ng, N. L., Kroll, J. H., Chan, A. W. H., Chhabra, P. S., Flagan, R. C., and Seinfeld, J. H.: Secondary organic aerosol formation from m-xylene, toluene, and benzene, Atmos. Chem. Phys., 7, 3909–3922, https://doi.org/10.5194/acp-7-3909-2007, 2007.

Noda, J., Volkamer, R., and Molina, M. J.: Dealkylation of alkylbenzenes: a significant pathway in the toluene, o-, m-, p-xylene plus OH reaction, J. Phys. Chem. A, 113, 9658–9666, https://doi.org/10.1021/jp901529k, 2009.

Orlando, J. J., Tyndall, G. S., and Wallington, T. J.: The atmospheric chemistry of alkoxy radicals, Chem. Rev., 103, 4657–4690, https://doi.org/10.1021/cr020527p, 2003.

Palm, B. B., Campuzano-Jost, P., Ortega, A. M., Day, D. A., Kaser, L., Jud, W., Karl, T., Hansel, A., Hunter, J. F., Cross, E. S., Kroll, J. H., Peng, Z., Brune, W. H., and Jimenez, J. L.: In situ secondary organic aerosol formation from ambient pine forest air using an oxidation flow reactor, Atmos. Chem. Phys., 16, 2943–2970, https://doi.org/10.5194/acp-16-2943-2016, 2016.

Peng, Z., Day, D. A., Ortega, A. M., Palm, B. B., Hu, W., Stark, H., Li, R., Tsigaridis, K., Brune, W. H., and Jimenez, J. L.: Non-OH chemistry in oxidation flow reactors for the study of atmospheric chemistry systematically examined by modeling, Atmos. Chem. Phys., 16, 4283–4305, https://doi.org/10.5194/acp-16-4283-2016, 2016.

Peng, Z., Palm, B. B., Day, D. A., Talukdar, R. K., Hu, W. W., Lambe, A. T., Brune, W. H., and Jimenez, J. L.: Model evaluation of new techniques for maintaining high-NO conditions in oxidation flow reactors for the study of OH-initiated atmospheric chemistry, ACS Earth Space Chem., 2, 72–86, https://doi.org/10.1021/acsearthspacechem.7b00070, 2018.

Rissanen, M. P., Kurtén, T., Sipilä, M., Thornton, J. A., Kangasluoma, J., Sarnela, N., Junninen, H., Jørgensen, S., Schallhart, S., Kajos, M. K., Taipale, R., Springer, M., Mentel, T. F., Ruuskanen, T., Petäjä, T., Worsnop, D. R., Kjaergaard, H. G., and Ehn, M.: The formation of highly oxidized multifunctional products in the ozonolysis of cyclohexene, J. Am. Chem. Soc., 136, 15596–15606, https://doi.org/10.1021/ja507146s, 2014.

Rissanen, M. P.: NO_2 suppression of autoxidation-inhibition of gas-phase highly oxidized dimer product formation, ACS Earth Space Chem., 2, 1211–1219, https://doi.org/10.1021/acsearthspacechem.8b00123, 2018.

Sarnela, N., Jokinen, T., Duplissy, J., Yan, C., Nieminen, T., Ehn, M., Schobesberger, S., Heinritzi, M., Ehrhart, S., Lehtipalo, K., Tröstl, J., Simon, M., Kürten, A., Leiminger, M., Lawler, M. J., Rissanen, M. P., Bianchi, F., Praplan, A. P., Hakala, J., Amorim, A., Gonin, M., Hansel, A., Kirkby, J., Dommen, J., Curtius, J.,

Smith, J. N., Petäjä, T., Worsnop, D. R., Kulmala, M., Donahue, N. M., and Sipilä, M.: Measurement–model comparison of stabilized Criegee intermediate and highly oxygenated molecule production in the CLOUD chamber, Atmos. Chem. Phys., 18, 2363–2380, https://doi.org/10.5194/acp-18-2363-2018, 2018.

Sato, K., Takami, A., Kato, Y., Seta, T., Fujitani, Y., Hikida, T., Shimono, A., and Imamura, T.: AMS and LC/MS analyses of SOA from the photooxidation of benzene and 1,3,5-trimethylbenzene in the presence of NO_x: effects of chemical structure on SOA aging, Atmos. Chem. Phys., 12, 4667–4682, https://doi.org/10.5194/acp-12-4667-2012, 2012.

Schwantes, R. H., Schilling, K. A., McVay, R. C., Lignell, H., Coggon, M. M., Zhang, X., Wennberg, P. O., and Seinfeld, J. H.: Formation of highly oxygenated low-volatility products from cresol oxidation, Atmos. Chem. Phys., 17, 3453–3474, https://doi.org/10.5194/acp-17-3453-2017, 2017.

Seinfeld, J. H. and Pandis, S. N.: Atmospheric Chemistry and Physics: From Air Pollution to Climate Change, Third Edition, John Wiley and Sons, Inc., Hoboken, New Jersey, 2016.

Tsiligiannis, E., Hammes, J., Salvador, C. M., Mentel, T. F., and Hallquist, M.: Effect of NO_x on 1,3,5-trimethylbenzene (TMB) oxidation product distribution and particle formation, Atmos. Chem. Phys., 19, 15073–15086, https://doi.org/10.5194/acp-19-15073-2019, 2019.

Wang, L. M., Wu, R. R., and Xu, C.: Atmospheric oxidation mechanism of benzene. fates of alkoxy radical intermediates and revised mechanism, J. Phys. Chem. A, 117, 14163–14168, https://doi.org/10.1021/jp4101762, 2013.

Wang, M., Chen, D., Xiao, M., Ye, Q., Stolzenburg, D., Hofbauer, V., Ye, P., Vogel, A. L., Mauldin, R. L., Amorim, A., Baccarini, A., Baumgartner, B., Brilke, S., Dada, L., Dias, A., Duplissy, J., Finkenzeller, H., Garmash, O., He, X.-C., Hoyle, C. R., Kim, C., Kvashnin, A., Lehtipalo, K., Fischer, L., Molteni, U., Petäjä, T., Pospisilova, V., Quéléver, L. L. J., Rissanen, M., Simon, M., Tauber, C., Tomé, A., Wagner, A. C., Weitz, L., Volkamer, R., Winkler, P. M., Kirkby, J., Worsnop, D. R., Kulmala, M., Baltensperger, U., Dommen, J., El-Haddad, I., and Donahue, N. M.: Photo-oxidation of aromatic hydrocarbons produces low-volatility organic compounds, Environ. Sci. Technol., 54, 7911–7921, https://doi.org/10.1021/acs.est.0c02100, 2020.

Wang, S., Wu, R., Berndt, T., Ehn, M., and Wang, L.: Formation of highly oxidized radicals and multifunctional products from the atmospheric oxidation of alkylbenzenes, Environ. Sci. Technol., 51, 8442–8449, https://doi.org/10.1021/acs.est.7b02374, 2017.

Wang, Y., Mehra, A., Krechmer, J. E., Yang, G., Hu, X., Lu, Y., Lambe, A., Canagaratna, M., Chen, J., Worsnop, D., Coe, H., and Wang, L.: Oxygenated products formed from OH-initiated reactions of trimethylbenzene: autoxidation and accretion, Atmos. Chem. Phys., 20, 9563–9579, https://doi.org/10.5194/acp-20-9563-2020, 2020.

Wu, R., Pan, S., Li, Y., and Wang, L.: Atmospheric oxidation mechanism of toluene, J. Phys. Chem. A, 118, 4533–4547, https://doi.org/10.1021/jp500077f, 2014.

Xu, L., Møller, K. H., Crounse, J. D., Kjaergaard, H. G., and Wennberg, P. O.: New insights into the radical chemistry and product distribution in the OH-initiated oxidation of benzene, Environ. Sci. Technol., 54, 13467–13477, https://doi.org/10.1021/acs.est.0c04780, 2020.

Yu, J. Z. and Jeffries, H. E.: Atmospheric photooxidation of alkylbenzenes-I I. Evidence of formation of epoxide intermediates, Atmos. Environ., 31, 2281–2287, https://doi.org/10.1016/s1352-2310(97)88637-2, 1997.

Yu, J. Z., Jeffries, H. E., and Sexton, K. G.: Atmospheric photooxidation of alkylbenzenes- I. Carbonyl product analyses, Atmos. Environ., 31, 2261–2280, https://doi.org/10.1016/s1352-2310(97)00011-3, 1997.

Zaytsev, A., Breitenlechner, M., Koss, A. R., Lim, C. Y., Rowe, J. C., Kroll, J. H., and Keutsch, F. N.: Using collision-induced dissociation to constrain sensitivity of ammonia chemical ionization mass spectrometry (NH_4^+ CIMS) to oxygenated volatile organic compounds, Atmos. Meas. Tech., 12, 1861–1870, https://doi.org/10.5194/amt-12-1861-2019, 2019a.

Zaytsev, A., Koss, A. R., Breitenlechner, M., Krechmer, J. E., Nihill, K. J., Lim, C. Y., Rowe, J. C., Cox, J. L., Moss, J., Roscioli, J. R., Canagaratna, M. R., Worsnop, D. R., Kroll, J. H., and Keutsch, F. N.: Mechanistic study of the formation of ring-retaining and ring-opening products from the oxidation of aromatic compounds under urban atmospheric conditions, Atmos. Chem. Phys., 19, 15117–15129, https://doi.org/10.5194/acp-19-15117-2019, 2019b.

Zhao, Y., Thornton, J. A., and Pye, H. O. T.: Quantitative constraints on autoxidation and dimer formation from direct probing of monoterpene-derived peroxy radical chemistry, P. Natl. Acad. Sci. USA, 115, 12142–12147, https://doi.org/10.1073/pnas.1812147115, 2018.

Zheng, Y., Cheng, X., Liao, K., Li, Y., Li, Y. J., Huang, R.-J., Hu, W., Liu, Y., Zhu, T., Chen, S., Zeng, L., Worsnop, D. R., and Chen, Q.: Characterization of anthropogenic organic aerosols by TOF-ACSM with the new capture vaporizer, Atmos. Meas. Tech., 13, 2457–2472, https://doi.org/10.5194/amt-13-2457-2020, 2020.

Ziemann, P. J., and Atkinson, R.: Kinetics, products, and mechanisms of secondary organic aerosol formation, Chem. Soc. Rev., 41, 6582–6605, https://doi.org/10.1039/C2CS35122F, 2012.